International Journal of Nanoelectronics and Materials
Volume 14 (Special Issue) December 2021 [1-10]

Effect of Spinning Rate on the Performance of Multilayer Bi-perovskite Solar Cells

M.F. Achoi[1,2*], S. Aiba[1], S. Kato[1], N. Kishi[1] and T. Soga[1*]

[1]Department of Electrical and Mechanical Engineering, Nagoya Institute of Technology, Showa-ku, Gokiso-cho, Nagoya, Aichi 466-8555, Japan
[2]Faculty of Applied Sciences, Universiti Teknologi MARA, Cawangan Sabah, Kampus Kota Kinabalu, Sabah 88997, Malaysia

ABSTRACT

Multilayer methylammonium bismuth iodide perovskite solar cells (Bi-PeSC's) were fabricated using multi-step spin coating by changing the spinning rates from 500 rpm to 5000 rpm with keeping the layer number at eight. The aim of this work is to study the effect of spinning rates on the multilayer Bi-PeSC's performance. The SEM result shows the improved morphological properties at an optimum speed of spinning. At the same time, the XRD analysis exhibits that a very strong intensity and a narrow peak of MBI are observed at 12.67° (101) of 500 rpm, and it completely disappeared at 5000 rpm. The Dektak measurement showed that the thickness of multilayer Bi-PeSC's is reduced from 600 nm to 300 nm as the spinning rates increased from 500 rpm to 5000 rpm. Furthermore, the multilayer Bi-PeSC's showed an increment in the open circuit voltage with a maximum of 0.42V at an optimum spinning rate of 1000 rpm. The Bi-PeSC's performance improvement is attributed to the formation of a moderate thickness of 568 nm. In brief, the spinning rate significantly influences the morphology, optical and structural properties of multilayer Bi-PeSC's. In the future development of Bi-PeSC's device, our research's finding might have an appreciated contribution towards a better improvements of solar cells performance.

Keywords: Bismuth-perovskite, Perovskite solar cells, Multi-step spin coating

1. INTRODUCTION

Up to date, the bismuth-based perovskite materials with the chemical formula ($A_3Bi_2X_9$; A= $CH_3NH_3^+$, X=halide group) have great much attention for solar cells device application. Hence, many methods or techniques have been initiated by the previous researcher, such as chemical vapor deposition [1], spray deposition [2], thermal evaporation [3], inkjet printing [4], doctor blade [5], and slot-dye coating [6]. All those developed methods have the same aim to be achieved is to improve the performance of solar cell devices-based perovskite material. Besides, to obtain a good quality of an absorber layer in heterojunction design of solar cells device, with optimum criteria of a layer such as surface uniformity, coverages [7], optimized thickness [8,9], defect and pinhole-free [10]. In this regard, the methylammonium bismuth iodide (MBI) is widely discovered by many researchers due to non-toxic material compared to Pb, chemically stable and environment friendly for lead-free perovskite solar cells (PeSC's) [11]. However, up to date, the MBI surface morphology and its performance are still compromised. Thus, the material parameters to the thickness of a MBI layer may affect the morphology and Bi-PeSC's performance. This is because the thickness of a layer might contribute to other effects such as surface uniformity and coverage area. Jeon et al. reported that the performance of solar cells dropped significantly because the surface uniformity and coverages were poor [7]. Besides, Heo et al. and Burschka et al. reported that a thick film resulted in uniformity of a film with 100% surface coverage on the mp-TiO_2 [12,13]. At the same time, Eperon et al. reported that a thicker layer could transfer more electronic charge to the perovskite [14]. On the contrary, according to Xiao et al. the thicker perovskite layer can be detrimental to PeSC's performance [15].

*faizalachoi86@gmail.com, soga@nitech.ac.jp

Therefore, our motivation to obtain moderate thickness between 300-600 nm with varying spinning rate was investigated.

Furthermore, the spin-coating method is well-known solution-processing with a low-cost method for thin-film solar cells fabrication [16]. In this work, we employed a new modification method from spin-coating method, an all-solution processed multi-step spin coating technique. This method gives promising production of absorber layer with ease and short time. Moreover, the poor coverage and uniformity of thin-film solar cells can be resolved by this method [17,18,19]. Herein, we report the preparation of eight layers of MBI perovskite with varying spinning rates using all-solution processed multi-step spin coating for the first time. As far as our concern, there are no reports on this parameter for multilayer Bi-PeSC's prepared using this method. Besides, the effect of the spinning rate on the thickness of the MBI layer is also presented. At the end of this work, the absorber layer thickness and spinning rate are optimized.

2. MATERIAL AND METHODS

First, the preparation of c-TiO_2 as an electron transport layer (ETL) was prepared according to our previous method in ref. [20]. While mp-TiO_2 was prepared by diluting 0.04687g of P25 TiO_2 in 10 mL of 1-butanol. Then, the mp-TiO_2 is annealed at 500^{o}C for 1 h. For making 0.5M MBI solution, both precursors (BiI_3 and MAI) were mixed according to our previously reported work [21]. The MBI solution was spin-coated at 500 rpm for 8 times on the TiO_2 surface to obtain 8 layers of MBI. At intervals between each layer fabrication, the MBI layer was dried at 100^{o}C for 10 min. After the whole 8 layers fabrication, the MBI layer left for the cooling process for 5 min. This fabrication step is repeated for 1000, 3000 and 5000 rpm sample. Next, as a hole transport layer (HTL), the P3HT was dissolved in dichlorobenzene, so that the concentration of P3HT is 15 $mg.mL^{-1}$. The P3HT solution was spin-coated at 3000 rpm for 20 s and then annealed on a hot plate at 120^{o}C for 15 min. The whole fabrication process of the MBI layer was carried out in a dry nitrogen-filled glovebox. Finally, the colloidal graphite was spin-coated on top of the P3HT layer at 5000 rpm for 20 s and cooled at room temperature, followed by the deposition of Ag paste. The Ag paste is then left in a room temperature for drying. The purpose of using a colloidal graphite is to connect P3HT and silver electrode smoothly [22]. It is same function as a gold electrode which has been widely used in solar cells fabrication as before. Besides, graphite is a good conductivity of material.

For the characterization part, the structural properties of multilayer MBI were characterized using (XRD; Rigaku RINT-2100 diffractometer) while the surface morphology is characterized using (SEM; JEOL JSM-7600F). Next, an optical absorption property is characterized using a UV-Vis spectrophotometer (JASCO Model V-570). Finally, the thicknesses of a layer were measured using the Dektak machine (Veeco-Dektak150) and the solar cells performance were measured using a solar simulator under simulated solar light illumination (AM 1.5, 100 $mW.cm^{-2}$).

3. RESULTS AND DISCUSSION

3.1 XRD analysis

Figure 1 indicates the XRD curves of multilayer Bi-perovskite at different spinning rates. At 500 rpm, five peaks of MBI are observed at 12.67^o, 14.40^o, 16.40^o, 24.58^o, and 29.38^o, which are assigned to (101), (102), (004), (006), and (204) lattice planes, respectively [9,23,24,25,26]. Other MBI peaks are detected at 32.29^o, 43.37^o, and 44.76^o, which is the same as MBI peaks reported in ref. [1]. Two peaks at 29.60^o and 31.7^o, corresponding to the (012) and (110) lattice planes, are assigned to Bi_2O_3 and BiOI, respectively [9,23]. These two compounds are formed in MBI layer due to the air exposure during fabrication process as Hoye et al. reported [9]. While

another three peaks of FTO were observed at 26.82° [25], 33.91° [24], and 38.06° [27]. At 500 rpm, three MBI peaks are observed at 24.58° (006), which appeared as a strong intensity and very narrow peak, while another two peaks at 12.67° (101) and 16.40° (004) have appeared as the intense peak. However, the MBI peak at 24.58° (006) and 12.67° (101) slowly decreased in intensity. Afterward, the peak at 12.67° (101) is completely disappeared at 3000 rpm and 5000 rpm. While peak at 24.58° (006) became a bit less intense and broad peak than TiO_2 peak at 25.37° [26]. Interestingly, it can be seen that at the beginning of the spinning rate, the MBI peak at 24.58° (006) appeared as a very strong intensity than TiO_2. After that this peak became a less intense peak than the TiO_2 peak at 5000 rpm, and at the same time, FTO peaks at 33.91° [24], and 38.06° [27] conquered dominantly with very intense and narrow peak than earlier seen of two FTO peaks, which very low intensity and broad peak. All these elucidate that the MBI layer became a thin layer while some of the layer surfaces are non-uniform and are not well covered at 5000 rpm as shown in Figure 2 and 3(d). Moreover, the peak intensity of the FTO is increased due to the thin perovskite layer. According to Jeon et al. the uniformity of the perovskite films depended on the thickness of a layer [7] while Eperon et al. mentioned that 100% surface coverage of a layer depended on the spinning condition [14].

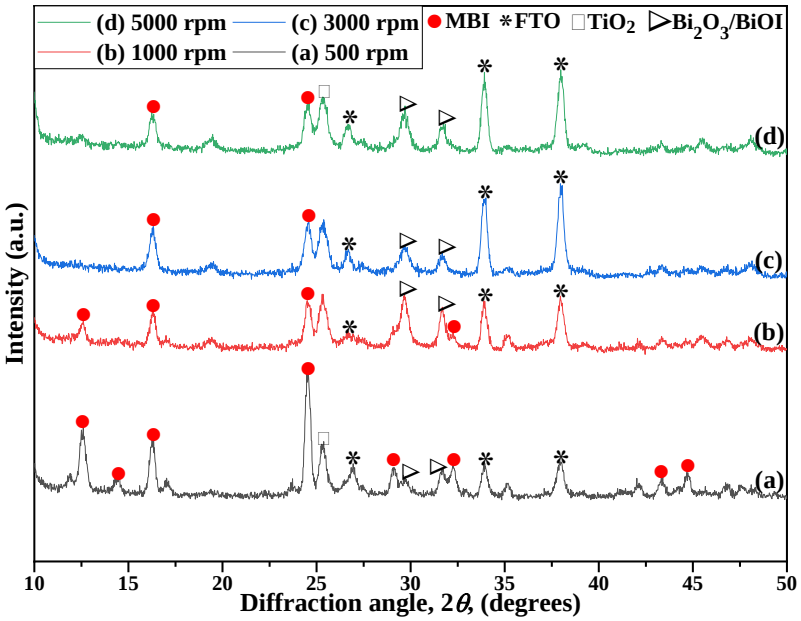

Figure 1. The XRD peaks of the multilayer Bi-PeSC's at different spinning rates.

Furthermore, we calculate the crystallite size using Scherrer's equation [25]. It shows that at 500 rpm, the crystallite size (*D*) is 44 nm. After that, at a speed ≥ 1000 rpm, we found that the *D* value of the MBI layer is drastically decreased. The *D* values recorded are 36 nm, 22 nm, and 11 nm for 1000 rpm, 3000 rpm and 5000 rpm, respectively. It means that the MBI particles do not have enough time to be deposited well on the TiO_2 surface, especially at 5000 rpm. In other words, the MBI particles are not accumulated and formed an agglomerated particle, as visually confirmed by inset SEM images in Figure 3(d). The agglomeration happens due to the crystallization process once applying heat to promote grain growth as reported by Thompson et al. [28]. This will be further described later in SEM morphology properties section. In brief, as the spinning rates changed from 500 rpm to 5000 rpm, the MBI peaks at 12.67° (101) is drastically decreased and then completely disappeared. While the FTO peak at 33.91° [24] and 38.06° [27] were appeared dominantly and became a strong and intense peak. It means that the MBI layer became less thick at 5000 rpm, as proof, we have measured the thickness of the MBI layer using the Dektak measurement, where the recorded thicknesses are shown in Figure 2. This indicated that the layer thickness decreases accordingly with the *D* value as the spinning

rates increased, as shown in Figure 2. The influence of *D* on the J_{sc} and the performance of Bi-PeSC's will be discussed in the next solar cell performance section.

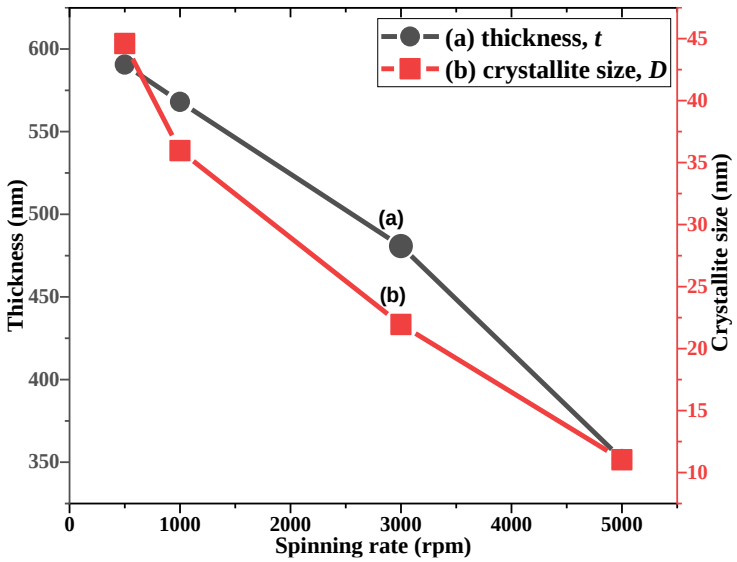

Figure 2. The variation of thickness and crystallite size against spinning rate.

3.2 Surface morphology properties

Figure 3 illustrates the SEM morphology of multilayer Bi-PeSC's at different spinning rates. At 500 rpm, the MBI layer is not uniformly distributed but accumulated and agglomerated MBI particles are formed as confirmed by the XRD result in Figure 3(a). Thus, many big-size particles in white colour were formed, as illustrated in inset Figure 3(a). According to Chen et al. the formation of big-sized particles is due to the nucleation and crystallization process [29]. At doubled spinning rate to 1000 rpm, the SEM image illustrated a small MBI particles start to randomly distribute uniformly, and then covered throughout the TiO_2 surface as shown in inset Figure 3(b). In addition, no agglomeration particle is seen on the TiO_2 surface. However, at 3000 rpm, SEM images in Figure 3(c) visually depict that the MBI particles start to be distributed far away, and the surface is not well covered. Finally, at 5000 rpm, the MBI particles are not well uniformly distributed with a space between white particles, and some of the particles are discretely accumulated and focus to one spot location, as shown in Figure 3(d). It means that the particle is not stick together during spin coating. Instead, the particles move aside from a layer and then agglomerate as an abundant island, as visually depicted in inset Figure 3(d). Jeon et al. reported that during spin coating, the present of centrifugal force applied from the rotation of the spin coating rotor made the solution convective spreading flow [7]. However, this centrifugal force became high as the spinning rate increases, spreading the solution too fast. It finally deteriorating the surface morphology of MBI resulting in the non-homogeneity layer.

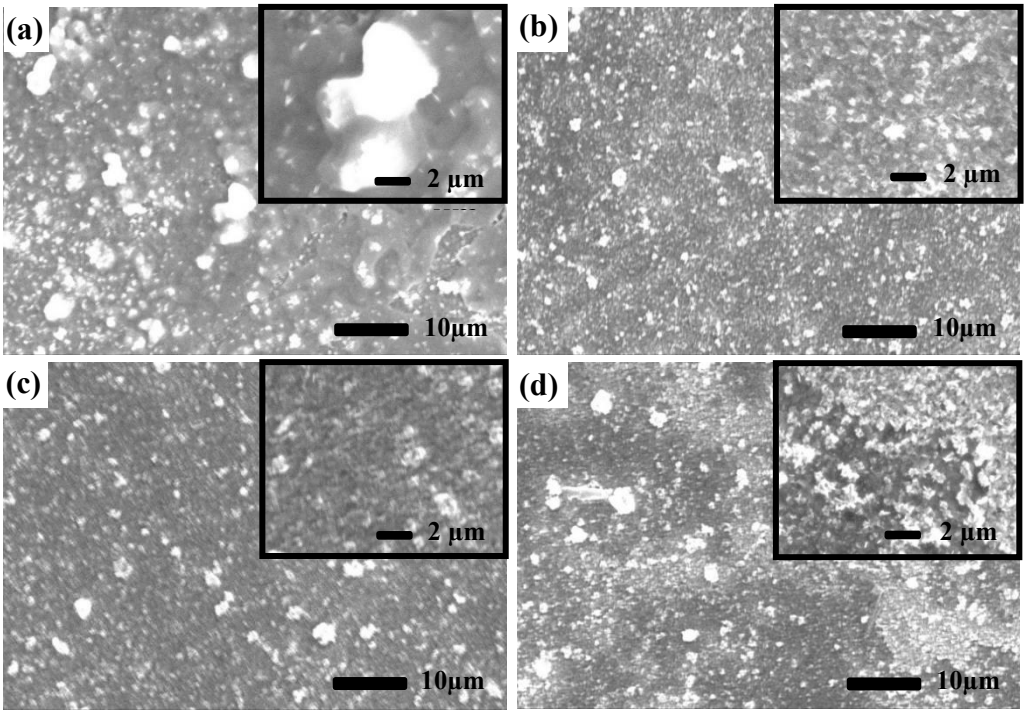

Figure 3. SEM morphology of the multilayer MBI at different spinning rates: (a) 500 rpm, (b) 1000 rpm, (c) 3000 rpm, and (d) 5000 rpm. Inset pictures are magnified morphology.

3.3 Optical properties

Figure 4 shows the absorbance of Bi-PeSC's characterized using a UV-visible spectrophotometer in the UV-visible region. Generally, all the MBI layers shows that the light absorption peak is around 500 nm in the visible region. The optical bandgap is around 2.0eV - 2.13eV. The UV-visible absorption indicates that the different absorbance intensity while the optical band gap energy is changed a bit. At a low speed of 500 rpm and 1000 rpm, the recorded absorbance intensity is higher than 3000 rpm and 5000 rpm. In accordance with SEM images Figure 3((a) and (b)) indicates that the multilayer MBI with good uniformity and well covered surface has a good absorption. Moreover, the thickness that earlier discussed influenced the absorption of light as well. In accordance to Figure 2, the thicker layer at low speed, shows the higher light absorption as shown in Figure 4((a) and (b)). Instead, the thinner layer at higher spinning rate causes the lower light absorption as shown in Figure 4((c) and (d)). This might happen due to the detrimental effect of the MBI thickness on light absorption. According to Chen et al. increasing the thickness of films resulted in the high light absorption benefits with the filling of the MBI [29]. Besides, Eperon et al. reported that incomplete coverage area of the perovskite surface resulted in loss of light absorption in the solar cells [14], as indicated in the Figure 3(d) and 4(d). Therefore, the MBI layer at 500 rpm and 1000 rpm have a strong absorbance intensity, thus enhancing the light-harvesting property of the multilayer Bi-PeSC's device. The influence of the absorption and the thickness of the MBI layer on the solar cell's performance will be discussed in the next solar cell performance section.

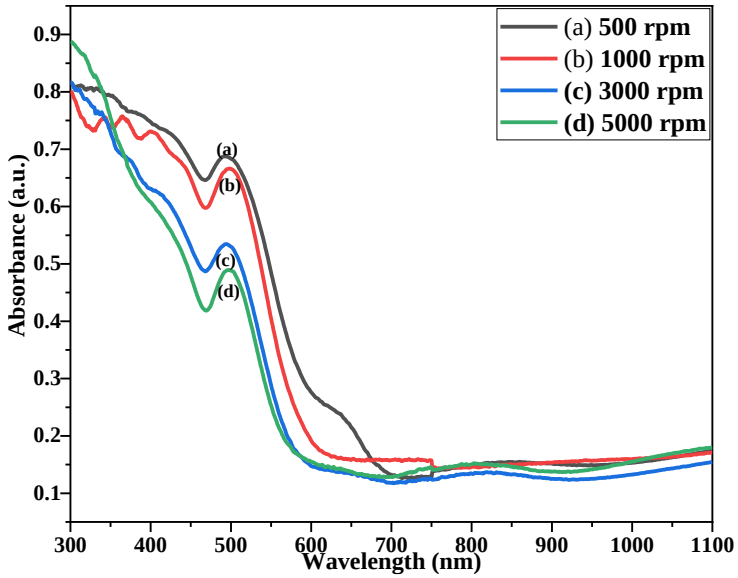

Figure 4. The optical absorbance of the multilayer MBI at different spinning rates.

3.4 Solar cell's performance

Figure 5 shows the corresponding current density-voltage curves of Bi-PeSC's under the solar simulator and Figure 6(a) shows the relationship of short circuit current (J_{sc}) and open circuit voltage (V_{oc}) with the spinning rates, while Figure 6(b) illustrates the schematic diagram of the solar cell. Figure 5(a) indicates that at 500 rpm the current density and voltage is very low compared to others spinning rates. This is due to a low spinning rate leads to agglomerated particles and a thicker layer. Consequently, the contact area between the hole transport layer (HTL) and electron transport layer (ETL) was reduced. Hence, it produces a shunt paths leading to the current leakage as reported by Snaith et al. [30]. As for increased spinning speed to 1000 rpm, we found that the maximum voltage was recorded at 0.42V and PCE is 0.034% with an optimized thickness of the MBI layer at 568 nm. Our finding agrees that Chen et al. found that 564 nm of MBI film shows better performance of solar cell devices. They suggest that 564 nm of MBI film might be more efficient for the electron extraction at the TiO_2/perovskite interface, and then the photoexcited electron can be transferred easily from the MBI to the TiO_2 layer [29]. Moreover, moderate thickness contributes to a good PCE, which may reduce the recombination of charge carriers. As a result, the charge carriers can be easily extracted before the recombination happen. Besides, Zhao et al. reported that the thickness of an MBI layer might affect to the charge diffusion length, hence, it influences the photovoltaic performance [31]. It thus elucidates that the thickness relying on the spinning rate influenced the performance of multilayer Bi-PeSC's as shown in Figure 2. The performance of multilayer Bi-perovskite is drastically decreased according to the spinning rate which exhibits 0.18V and 0.09V, for 3000 rpm and 5000 rpm, respectively, as shown in Figure 6(a). In accordance with the inset Figure 3(d), non-uniformity morphology with lack of coverages area of MBI layer surface contributed to the current leakage while the thickness also influences the performance of solar cells as well. According to Eperon et al. the lowest coverages contribute the lowest efficiencies of the solar cells [14]. This explanation agreed with our findings as shown in Figure 3(d) and inset Table 1 of Figure 5.

Furthermore, the *D* value is relying on the spinning rates that affected Bi-PeSC's performance. It is shown that the performance decreases accordingly as shown in Figure 6(a) and then the *D* values and the thickness were decreased along with the spinning rates as shown in Figure 2. In the inset Table of Figure 5 it can be seen that the J_{sc} decreases with *D* value, which means high spinning rate with a less thick layer of MBI of 352 nm creates the small size of crystallite size

(11 nm) resulting in a small J_{sc} value because the structural defect density is increased as shown in Figure 2. After 1000 rpm, the performance of solar cells decreases as well. This elucidates that the spinning rates influences the thickness, crystallite size and the performances of the Bi-PeSC's. On the other hand, *D* became small, as seen in the inset Figure 3(d), while a non-uniform surface at high speed of spinning causes the current leakage and the current recombination is increased. Consequently, the V_{oc} and J_{sc} became low, as stated in the inset Table of Figure 5. Besides, a better interface layer attributed to the improved morphology of MBI layer leads to V_{oc} is increased as reported by Ataei et al. [32]. According to Sanders et al. the reduction of interface area in a surface layer can hamper the extraction of charge carriers as reported by [1]. Besides, Eperon et al. reported that a uniform perovskite thin film with good surface coverages give the best output voltages [13].

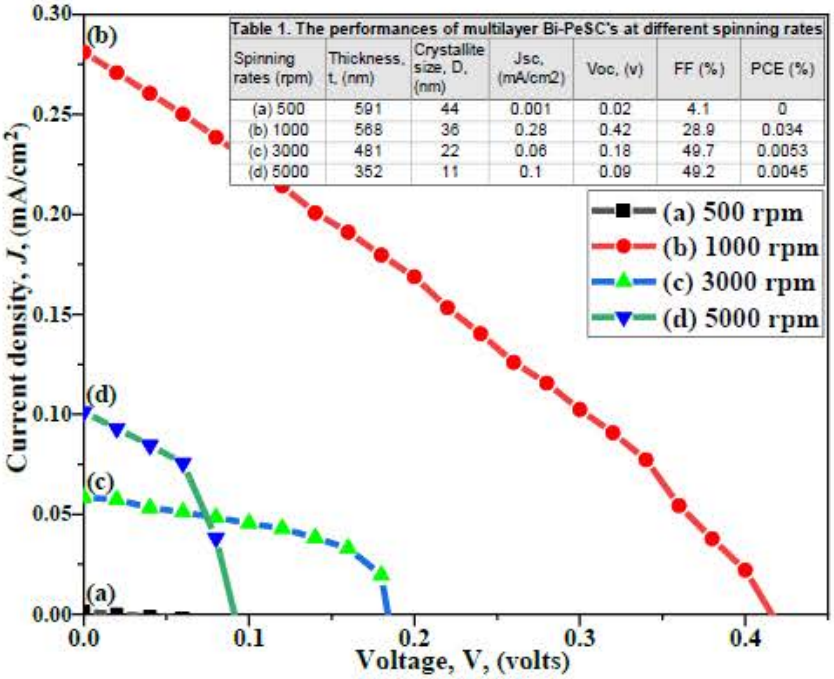

Figure 5. The I-V performance of multilayer Bi-perovskite solar cell at different speeds of spin-coating. The inset table shows the summary of solar cell parameters.

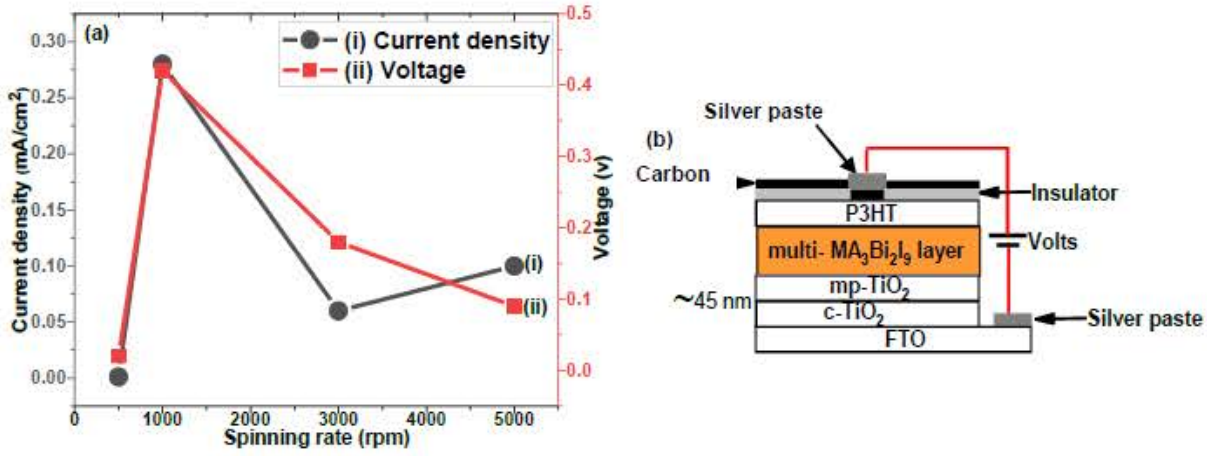

Figure 6. (a) The variation of current density and voltage versus spinning rate, and (b) the structure of the solar cell of multilayer Bi-perovskite solar.

4. CONCLUSION

In summary, we have successfully fabricated the Bi-PeSC's using all-solution processed multi-step spin coating method at different spinning rates. We found that the spinning rate significantly influenced the thickness, crystallinity, crystal size, surface coverage and the uniformity of multilayer Bi-PeSC's. The Dektak measurement and XRD analysis shows that the optimized thickness and crystallite size of a MBI layer are 568 nm and 36 nm, respectively, while, from the photovoltaic result shows that the improved Bi-PeSC's performance contributed to the J_{sc} of 0.28 mA/cm^2, V_{oc} of 0.42V, fill factor of 29% and the PCE of 0.034% for the optimum spinning rate at 1000 rpm. However, low speed is not better because a thicker layer is produced, which causes the mobility charge carrier poor, while too-fast spinning rate is also not reasonable because it leads to a thin layer which produces current leakage and increased the charge-carrier recombination and finally resulted in the poor performance of Bi-PeSC's. Therefore, it is very important to control the spinning rate to obtain a better morphology, an ideal thickness and good UV-visible absorption, which will lead to the better improvement of Bi-PeSC's performance.

ACKNOWLEDGEMENTS

The author would like to thank you to Japanese government (MEXT Scholarship) throughout this research work. Unforgettable to Universiti Teknologi MARA (UiTM) for supporting these studies.

REFERENCES

[1] S. Sanders, D. Stümmler, P. Pfeiffer, N. Ackermann, G. Simkus, M. Heuken, P. K. Baumann, A. Vescan, and H. Kalisch, "Chemical Vapor Deposition of Organic-Inorganic Bismuth-Based Perovskite Films for Solar Cell Application," Sci. Rep., vol. 9 (2019) pp. 9774.

[2] T. Mohammad, V. Kumar, and V. Dutta, "Electric field assisted spray coated lead-free bismuth iodide perovskite thin film for solar cell application," Sol. Energy., vol. 182 (2019) pp. 72–79.

[3] Z. Zhang, X. Li, X. Xia, Z. Wang, Z. Huang, B. Lei, and Y. Gao, "High-Quality $(CH_3NH_3)_3Bi_2I_9$ Film-Based Solar Cells: Pushing Efficiency up to 1.64%," J. Phys. Chem. Lett., vol. 8 (2017) pp. 4300–4307.

[4] F. Mathies, H. Eggers, B. S. Richards, G. Hernandez-Sosa, U. Lemmer, and U. W. Paetzold, "Inkjet-Printed Triple Cation Perovskite Solar Cells," ACS Appl. Energy Mater., vol. 1 (2018) pp. 1834–1839.

[5] K. Hwang, Y. S. Jung, Y. J. Heo, F. H. Scholes, S. E. Watkins, J. Subbiah, D. J. Jones, D. Y. Kim, and D. Vak, "Toward Large Scale Roll-to-Roll Production of Fully Printed Perovskite Solar Cells," Adv. Mater., vol. 27 (2015) pp. 1241–1247.

[6] T. M. Schmidt, T. Larsen-Olsen, J. E. Carlé, D. Angmo, and F. C. Krebs, "Upscaling of Perovskite Solar Cells: Fully Ambient Roll Processing of Flexible Perovskite Solar Cells with Printed Back Electrodes," Adv. Energy Mater., vol. 5 (2015) pp. 1500569.

[7] N. J. Jeon, J. H. Noh, Y. C. Kim, W. S. Yang, S. Ryu, and S. I. Seok, "Solvent engineering for high-performance inorganic-organic hybrid perovskite solar cells," Nat. Mater., vol. 13 (2014) pp. 897–903.

[8] T. Singh, Y. Udagawa, M. Ikegami, H. Kunugita, K. Ema, and T. Miyasaka, "Tuning of perovskite solar cell performance via low-temperature brookite scaffolds surface modifications," APL Mater., vol. 5 (2017) pp. 1.

[9] R. L. Z. Hoye, R. E. Brandt, A. Osherov, V. Stevanovic, S. D. Stranks, M. W. B. Wilson, H. Kim, A. J. Akey, J. D. Perkins, R. C. Kurchin, J. R. Poindexter, E. N. Wang, M. G. Bawendi, and V.

Bulovic, "Methylammonium Bismuth Iodide as a Lead-Free, Stable Hybrid Organic – Inorganic Solar Absorber," A Chem. Eur. J. Commun., vol. 80401 (2016) pp. 2605–2610.

[10] G. Dong, D. Xia, Y. Yang, L. Sheng, R. Fan, and L. Qiu, "Regulated Film Quality with Methylammonium Bromide Addition in a Two-Step Sequential Deposition to Improve the Performance of Perovskite Solar Cells," Energy Technol., vol. 5 (2017) pp. 1873–1879.

[11] M. F. Achoi, S. Aiba, S. Kato, N. Kishi, and T. Soga, "A novel approach towards compact and improved-crystallinity methylammonium bismuth iodide film via hot immersion method," Mater. Lett. X., vol. 12 (2021) pp. 100096.

[12] J. H. Heo, S. H. Im, J. H. Noh, T. N. Mandal, C. S. Lim, J. A. Chang, Y. H. Lee, H. J. Kim, A. Sarkar, M. K. Nazeeruddin, M. Grätzel, and S. I. Seok, "Efficient inorganic–organic hybrid heterojunction solar cells containing perovskite compound and polymeric hole conductors," Nat. Photonics., vol. 7 (2013) pp. 486–491.

[13] J. Burschka, N. Pellet, S. J. Moon, R. Humphry-Baker, P. Gao, M. K. Nazeeruddin, and M. Grätzel, "Sequential deposition as a route to high-performance perovskite-sensitized solar cells," Nature**,** vol. 499 (2013) pp. 316–319.

[14] G. E. Eperon, V. M. Burlakov, P. Docampo, A. Goriely, and H. J. Snaith, "Morphological control for high performance, solution-processed planar heterojunction perovskite solar cells," Adv. Funct. Mater., vol. 24 (2014) pp. 151–157.

[15] Z. Xiao, C. Bi, Y. Shao, Q. Dong, Q. Wang, Y. Yuan, C. Wang, Y. Gao, and J. Huang, "Efficient, high yield perovskite photovoltaic devices grown by interdiffusion of solution-processed precursor stacking layers," Energy Environ. Sci., vol. 7 (2014) pp. 2619–2623.

[16] Z. Yu and L. Sun, "Recent Progress on Hole-Transporting Materials for Emerging Organometal Halide Perovskite Solar Cells," Adv. Energy Mater., vol. 5 (2015) pp. 1500213.

[17] T. Singh, A. Kulkarni, M. Ikegami, and T. Miyasaka, "Effect of Electron Transporting Layer on Bismuth-Based Lead-Free Perovskite $(CH_3NH_3)_3Bi_2I_9$ for Photovoltaic Applications," ACS Appl. Mater. Interfaces., vol. 8 (2016) pp. 14542–14547.

[18] M. Lyu, J. H. Yun, M. Cai, Y. Jiao, P. V. Bernhardt, M. Zhang, Q. Wang, A. Du, H. Wang, G. Liu, and L. Wang, "Organic – inorganic bismuth (III)-based material: A lead- free, air-stable and solution-processable light-absorber beyond organolead perovskites," Nano Res., vol. 9 (2016) pp. 692–702.

[19] S. Sanders, D. Stümmler, P. Pfeiffer, N. Ackermann, F. Schimkat, G. Simkus, M. Heuken, P. K. Baumann, A. Vescan, and H. Kalisch, "Morphology Control of Organic–Inorganic Bismuth-Based Perovskites for Solar Cell Application," Phys. status solidi., vol. 215 (2018) pp. 1800409.

[20] M. F. b. Achoi, M. N. bt. Asiah, M. Rusop, and S. Abdullah, "The Effect of Growth Temperature on the Surface Properties of TiO_2 Nanostructures Grown on TiO_2 Templates," Trans. Mater. Res. Soc. Japan., vol. 36 (2011) pp. 273–279.

[21] M. F. Achoi, M. A. A. Noman, S. Kato, N. Kishi, and T. Soga, "Synthesis of bismuth triiodide nanofibers by spin-coating at room temperature," Materialia., vol. 16 (2021) pp. 101077.

[22] R. M. Matiur, S. Kato, and T. Soga, "All-solution-processed environment-friendly solid-state BiOI photovoltaic cell with high-short-circuit current by successive ionic layer adsorption and reaction (SILAR)," J. Mater. Sci. Mater. Electron., vol. 32 (2021) pp. 18342–18350.

[23] H. Li, C. Wu, Y. Yan, B. Chi, J. Pu, J. Li, and S. Priya, "Fabrication of Lead-Free $(CH_3NH_3)_3Bi_2I_9$ Perovskite Photovoltaics in Ethanol Solvent," ChemSusChem., vol. 10 (2017) pp. 3994–3998.

[24] D. Stümmler, S. Sanders, S. Mühlenbruch, P. Pfeiffer, G. Simkus, M. Heuken, A. Vescan, and H. Kalisch, "Fabrication of Methylammonium Bismuth Iodide Layers Employing Methylamine Vapor Exposure," Phys. Status Solidi A., vol. 216 (2019) pp. 1900169.

[25] Y. Shirahata, "Effects of annealing temperature on photovoltaic properties of lead-free $(CH_3NH_3)_3Bi_2I_9$ solar cells," J. Ceram. Soc. Japan., vol. 128 (2020) pp. 298–303.

[26] H. Wang, J. Tian, K. Jiang, Y. Zhang, H. Fan, J. Huang, L. M. Yang, B. Guan, and Y. Song, "Fabrication of methylammonium bismuth iodide through interdiffusion of solution-

processed BiI_3/CH_3NH_3I stacking layers," RSC Adv., vol. 7 (2017) pp. 43826–43830.

[27] Y. Wang, Y. Liu, Y. Xu, C. Zhang, H. Bao, J. Wang, Z. Guo, L. Wan, D. Eder, and S. Wang, "$(CH_3NH_3)_3Bi_2I_9$ perovskite films fabricated via a two-stage electric-field-assisted reactive deposition method for solar cells application," Electrochim. Acta., vol. 329 (2020) pp. 135173.

[28] C. V. Thompson, "Solid-state dewetting of thin films," Annu. Rev. Mater. Res., vol. 42 (2012) pp. 399–434.

[29] M. Chen, L. Wan, M. Kong, H. Hu, Y. Gan, J. Wang, F. Chen, Z. Guo, D. Eder, and S. Wang, "Influence of Rutile-TiO_2 nanorod arrays on Pb-free $(CH_3NH_3)_3Bi_2I_9$-based hybrid perovskite solar cells fabricated through two-step sequential solution process," J. Alloys Compd., vol. 738 (2018) pp. 422-431.

[30] H. J. Snaith, N. C. Greenham, and R. H. Friend, "The origin of collected charge and open-circuit voltage in blended polyfluorene photovoltaic devices," Adv. Mater., vol. 16 (2004) pp. 1640–1645.

[31] M. Zhang, H. Yu, M. Lyu, Q. Wang, J. H. Yun, and L. Wang, "Composition-dependent photoluminescence intensity and prolonged recombination lifetime of perovskite $CH_3NH_3PbBr_3$−x Clxfilms," Chem. Commun., vol. 50 (2014) pp. 11727–11730.

[32] M. Ataei, M. Adelifard, and S. S. Hosseini, "Physical Properties and Photovoltaic Performance of Perovskite Solar Cells Based on Lead-Free $A_3Bi_2I_9$ (A=CH_3NH_3, Cs) Active Layers," J. Electron. Mater., vol. 50 (2021) pp. 571–579.